Geometric criticality in scale-invariant networks

Lorenzo Lucarini [1,2] Giulio Cimini [1,2] and Pablo Villegas [2,3,*]

[1]*Physics Department and INFN, University of Rome Tor Vergata, 00133 Rome, Italy*

[2]*Enrico Fermi Research Center (CREF), 00184 Rome, Italy*

[3]*Instituto Carlos I de Física Teórica y Computacional, Universidad de Granada, 18071 Granada, Spain*

(Received 15 July 2025; accepted 26 January 2026; published 26 March 2026)

Dimension in physical systems determines universal properties at criticality. Yet, the impact of structural perturbations on dimensionality remains largely unexplored. Here, we characterize the attraction basins of structural fixed points in scale-invariant networks from a renormalization group perspective, demonstrating that basin stability connects to a structural phase transition. This topology-dependent effect, which we term *geometric criticality*, triggers a geometric breakdown hitherto unknown, which induces nontrivial fractal dimensions and unveils hidden Laplacian renormalization group flows toward unstable structural fixed points. Our systematic study of how networks and lattices respond to disorder paves the way for future analysis of nonergodic behavior induced by quenched disorder.

DOI: 10.1103/75gt-z6x6

I. INTRODUCTION

Topological shortcuts and structural sparsity shape complex dynamics across a broad spectrum of physical systems [1–3]. Shortcuts are key, for instance, in shaping brain functionality [4] or in improving the speed, efficiency, robustness, and functional diversity across neural networks [5–7]. Similar concepts pervade other areas, such as wormholes in general relativity [8] or wormhole attacks in wireless sensor networks [9]. In contrast, sparsity—for example, selective bond breaking in zeolites [10,11]—limits connectivity and tends to suppress large-scale organization. Vacancies—missing links in real materials—often compromise emergent phases by disrupting connectivity and collective behavior [3]. Such defects are known to modify electronic, magnetic, and structural properties in oxides, alloys, and skyrmion crystals [12–14]. Despite their relevance, understanding whether shortcuts and sparsity lead to structural transitions in complex systems remains a crucial open challenge.

In the context of complex networks, shortcuts were first formalized in the celebrated Watts-Strogatz (WS) model [15]. There, a simple ring lattice is "rewired" to introduce increasing amounts of disorder, allowing for a middle ground between regular and random networks while preserving high clustering and a very slowly growing diameter [16,17]. Extensions of the WS model, where the rewiring probability decays with distance, have further demonstrated that such shortcuts can modify the spectral dimension of the underlying graph [18]. However, do small-world effects merely induce smooth crossovers toward randomness or possibly lead to genuine structural phase transitions?

Dilute lattice models have long suggested that structural perturbations may influence universality classes [19]. Griffiths theoretically demonstrated that disordered systems could exhibit nonanalytic free energy over an extended temperature range [20]. Understanding Griffiths phases is essential for comprehending many other disordered systems, such as dilute ferroelectric materials [21,22]. However, no general framework has emerged to predict when and how such quenched disorder induces nonergodic behavior in arbitrary network architectures.

This motivated recent work on intrinsically scale-invariant networks, where structural fixed points were defined through the Laplacian renormalization group (LRG) [23]. This framework has introduced the notion of noninteger dimension tied to a constant entropy-loss rate across scales [24]. Crucially, this enables a distinction between scale-free and scale-invariant networks, with the latter admitting structural universality classes characterized by a well-defined *spectral dimension*, d_s. This global property of networks is related, for example, to the infrared singularity of the Gaussian process [25] and provides a robust generalization of the standard concept of Euclidean dimension for heterogeneous systems [25,26]. Furthermore, structural scale invariance leads to the emergence of characteristic strange attractors in reciprocal space, allowing the identification of hidden symmetries and local dimensionalities undetectable via standard methods [27]. Here, we exploit the LRG to address a fundamental question: Is it possible to define attraction basins for lattices and scale-invariant networks by exploring their response to topological perturbations?

We show that scale-invariant architectures under random perturbations (shortcut addition or link removal) exhibit previously unidentified structural phase transitions, which depend

*Contact author: pablo.villegas@cref.it

on the tiling patterns of the underlying structure. We term this phenomenon *geometric criticality*, as this topological phase transition corresponds to a geometric breakdown point where the system loses its well-defined dimension. This mechanism gives rise to highly heterogeneous, lacunar fractal networks and naturally defines an attraction basin for the LRG fixed points. Our framework provides a lens for analyzing the interplay between quenched disorder and dynamics, enabling a systematic exploration of how different perturbations alter the dimensional properties of the system itself.

II. STRUCTURAL FIXED POINTS

Topological scale-invariant structures were defined in Ref. [24], based on the LRG [23,28], which analyzes the spectral properties of the network Laplacian $\hat{L} = \hat{D} - \hat{A}$, where $\hat{A}$ is the adjacency matrix and $\hat{D}$ is the diagonal matrix of node degrees. Using the diffusion operator $e^{-\tau\hat{L}}$ as the evolution of a heat kernel at scale/diffusion time τ, one defines the Laplacian density matrix [29] $\hat{\rho}(\tau) = \frac{e^{-\tau\hat{L}}}{Z(\tau)}$, with $Z(\tau) = \mathrm{Tr}[e^{-\tau\hat{L}}]$, playing the role of a partition function [30]. This allows for a statistical mechanical description of the network structure, in which τ plays the role of inverse temperature and $\hat{L}$ acts as a Hamiltonian. The associated entropy $S(\tau) = -\mathrm{Tr}[\hat{\rho}(\tau)\log_{10}\hat{\rho}(\tau)]$ quantifies the effective number of active degrees of freedom at a given scale τ, decreasing from $S = \log_{10} N$ at $\tau = 0$ to $S = 0$ at $\tau \to \infty$. Its derivative with respect to $\log_{10}\tau$ defines the entropic susceptibility or heat capacity, $C(\tau) = -\frac{dS}{d\log_{10}\tau}$, which measures the rate of information loss as the system is coarse grained [23,30].

Scale invariance is defined by the condition that $C(\tau)$ remains constant across a broad range of scales, indicating the absence of a characteristic structural scale in the system [24]. This implies an entropy-loss rate proportional to the spectral dimension d_s, a global geometric quantity that generalizes the notion of Euclidean dimension to networks [25,26]. Hence, the presence of a plateau in the heat capacity, $C_0 = d_s/2$, reveals the spectral dimension d_s that characterizes the scale-invariant nature of homogeneous lattices or networks. Moreover, C usually presents small-scale resonant modes at short times, a signature of the elementary small-scale structure of the lattice or network [31], i.e., the ultraviolet cutoff Λ (in the jargon of the renormalization group). For a two-dimensional (2D) square lattice, this corresponds to the peak of C at $\tau \approx 1.24$ [black dashed line in Fig. 1(a)].

The second peak at larger values of τ instead reflects the whole lattice scale. In particular, the recent categorization of structural fixed points has shed light on four main classes of scale-invariant networks [24]: (1) regular lattices, (2) connected loopless networks, i.e., trees [32], (3) those with a nonvanishing clustering coefficient, as (u, v) flowers [33] [including the Dorogovtsev-Goltsev-Mendes (DGM) network [34]], and Kim and Holme networks [35], and (4) hierarchical modular networks (HMNs) originally proposed taking inspiration from brain networks [36].

The ordered set of Laplacian eigenvalues provides further geometric insight, as it represents network frequency modes analogous to the usual Fourier analysis [23,27]. Each eigenvalue represents a characteristic oscillation scale: Low

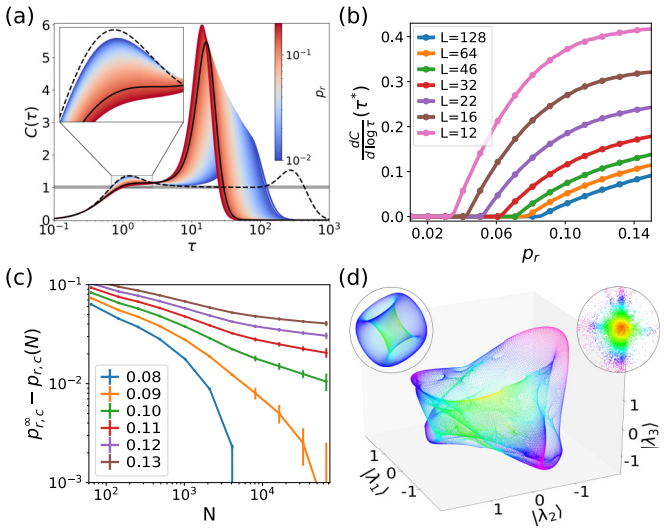

FIG. 1. Shortcuts in 2D square lattices. (a) Heat capacity, C, vs diffusion time, τ, for different rewiring probabilities (see colorbar, $L = 64$). The black dashed line corresponds to the unperturbed lattice. Inset: Close-up of the Λ region. (b) First derivative of the heat capacity at the first peak vs rewiring probability, p_r, for different lattice sizes (see legend). (c) Finite-size scaling analysis of the vanishing peaks in panel (b). The distance of the size-dependent peak locations $p_{r,c}(N)$ from their asymptotic value for $N \to \infty$, $p^{\infty}_{r,c}$, scales as a power law of the system size, only at $p^{\infty}_{r,c} = 0.10(1)$, revealing the existence of true scaling at criticality. (d) Low-dimensional representation using the three smallest low-frequency normalized network modes as the coordinate axes for a 2D square lattice of size $L = 256$. Parameters: $p_r = 2.3 \times 10^{-4}$, $p_r = 0$ (left inset), and $p_r = 0.1$ (right inset). All curves have been averaged over 10^3–10^5 realizations.

eigenvalues correspond to large-scale (low-frequency) modes, while high ones capture small-scale fluctuations (high frequencies). The spectral dimension inferred from entropy loss governs Laplacian embeddings, allowing any network to be unfolded into a low-dimensional manifold in κ space. Using the first n nontrivial Laplacian eigenvectors (for any connected network, the smallest eigenvalue, $\lambda_0 = 0$, is uniform and does not carry structural information), it is possible to map network nodes into $\mathbb{R}^n$, providing a geometric representation. In these embeddings, scale-invariant networks display attractorlike structures where the correlation dimension D matches the Euclidean dimension d_E for lattices, and $D = d_S/2$ for heterogeneous networks [27]. This provides a minimal and robust geometric representation just considering the minimum integer embedding dimension $d_E \geqslant D$ [27].

III. TOPOLOGICAL SHORTCUTS

We first consider the general case of regular lattices, where long-range connections are introduced by rewiring a fraction of the links. This is achieved by independently rewiring each link end point with probability p_r, while preserving the total number of edges in the network. Figure 1(a) shows the heat capacity as a function of the diffusion time for a 2D square network with varying rewiring probabilities. From now on, we consider the resulting giant component of the perturbed

structure. As the rewiring probability increases, the plateau in the heat capacity narrows, until the early-time heat capacity peak vanishes, signaling the breakdown of translational symmetry (see the saddle point on the solid black curve in the inset). Considering this first peak as a hallmark of lattice-scale order, we quantify this transition by examining the derivative of the heat capacity at the characteristic time of the first peak [see Fig. 1(b)]. Through finite-size scaling analyses, as reported in Fig. 1(c), we confirm the existence of a finite critical rewiring probability in the thermodynamic limit, $p_{r,c}^{\mathrm{sq}} = 0.10(1)$, which naturally defines the attraction basin of the 2D square lattice under the introduction of shortcuts. This geometric deformation can be further visualized using the three-dimensional (3D) Laplacian projection introduced above. As reported in Fig. 1(d), the 2D lattice becomes distorted due to long-range connections, leading to a collapsed Gaussian-like network at the critical value [see insets of Fig. 1(d) and Videos in the Supplemental Material [37]]. A similar behavior is observed for other regular lattices, such as 2D triangular and hexagonal lattices (see Appendix B), although with different critical rewiring thresholds: $p_{r,c}^{\mathrm{tr}} = 0.17(4)$ and $p_{r,c}^{\mathrm{hex}} = 0.055(10)$, respectively. Taken together, the disappearance of the short-scale peak in the heat capacity and the Gaussian collapse observed in Laplacian space constitute complementary signatures of a structural phase transition. These jointly define the limits of the attraction basin of the LRG structural fixed points.

IV. STRUCTURAL SPARSITY

We now turn to the role of link dilution, a classical model for quenched disorder known to influence critical behavior in various universality classes [19]. Starting from a regular lattice, we remove links randomly with probability p_d. Figure 2(a) displays the Laplacian embedding of a 2D square lattice at different values of p_d up to the percolation threshold, p_c, where the giant connected component disappears ($p_c = 0.5$ for the 2D square lattice), and a random tree (RT) structure emerges. This is a direct consequence of the Alexander-Orbach conjecture [38], which predicts that, at criticality, the giant component for isotropic percolation has a universal spectral dimension $d_s = 4/3$ across all dimensions.

The analysis of heat capacity versus dilution probability unveils a specific transition point, $p_{d,c}$, at which the ultraviolet cutoff Λ vanishes. Beyond this point, the effective dimension of the network decreases progressively toward the RT value $d_s = 4/3$ at p_c. We detect this geometric breakdown by analyzing the curvature (concavity) of the first peak in the heat capacity [see Fig. 2(b)], as illustrated in Fig. 2(c).

To better characterize this phase transition, we also compute the correlation integral as defined by Grassberger and Procaccia [27,39,40]. Using the projection of the ith node onto the d-dimensional space spanned by the first d nontrivial Laplacian eigenvectors, $\mathbf{x}_i = \sqrt{N}(\langle\lambda_1|i\rangle, \langle\lambda_2|i\rangle, \ldots, \langle\lambda_d|i\rangle)$, we can define the correlation integral in the reciprocal space as $C(\ell) = \frac{2}{N(N-1)} \sum_{i>j} \Theta(\ell - \|\mathbf{x}_i - \mathbf{x}_j\|) \sim \ell^D$, where Θ is the Heaviside step function. If the scaling law $C(\ell) \propto \ell^D$ holds, then D defines the network correlation dimension, which enables the detection of significant topological alterations in the

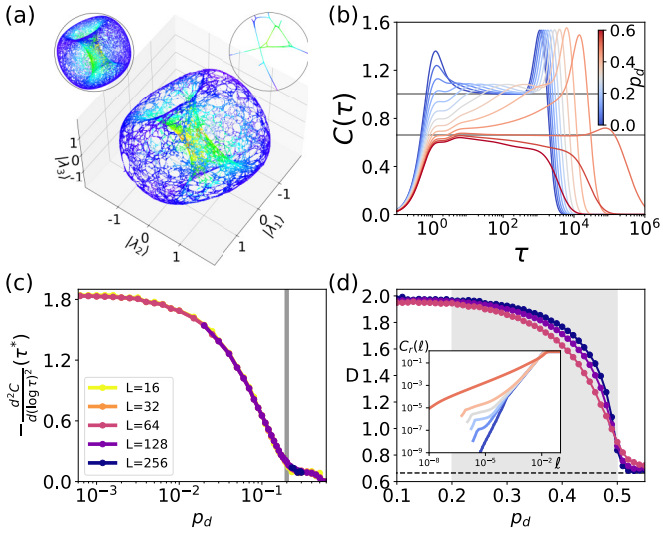

FIG. 2. Diluted 2D square lattices. (a) Low-dimensional representation using the three smallest low-frequency normalized network modes as the coordinate axes, for a lattice with $p_d = 0.35$, $p_d = 0.2$ (left inset), and $p_d = 0.5$ (right inset). (b) Heat capacity, C, vs diffusion time, τ, for different dilute probabilities (see colorbar). Gray lines represent the expected plateau for a 2D lattice and a RT. (c) Second derivative of the heat capacity at the first peak vs dilute probability, p_d, for different lattice sizes (see legend). The vertical gray line represents the point where the 2D ultraviolet cutoff is expected to disappear. (d) Estimated correlation dimension, D, vs dilution probability, p_d for different lattice sizes. Inset: Correlation integral $C(\ell)$ vs distance ℓ for different dilute probabilities. The gray area represents dilute probabilities between $p_{d,c}$ and the percolation threshold. All curves have been averaged over 10^3–10^4 realizations.

perturbed network. As shown in Fig. 2(d), D remains stable up to $p_{d,c}$; i.e., for low dilution, the lattice does not lose its bidimensional structure at large scale. From that point on, the dimensionality progressively decreases until it reaches the expected dimension for an RT. Both analyses capture the same phenomenon, yielding compatible estimates for the critical dilution probability $p_{d,c} = 0.20(5)$ for the 2D square lattice. Again, an equivalent behavior emerges for triangular and hexagonal lattices (see Appendix B), but with different critical points: $p_{d,c}^{\mathrm{tr}} = 0.25(1)$ and $p_{d_c}^{\mathrm{hex}} = 0.11(2)$, respectively. For 3D cubic lattices, we estimate a critical dilution threshold of $p_{d,c} = 0.55(5)$, while the rewiring threshold was found to be $p_{r,c} = 0.20(5)$ (see Appendix C). Note that performing correlation dimension analyses in the presence of shortcuts is considerably more challenging. While the method remains valid, the scaling region contracts, statistical noise increases, and extensive averaging becomes necessary. Moreover, the loss of spatial locality impairs the accuracy of Laplacian embeddings, making it more difficult to identify an effective embedding dimension. Conversely, in dilute models, it is another complementary measure that allows for the analysis of increasing system sizes, as it depends only on a few eigenvectors.

V. HETEROGENEOUS NETWORKS

We now extend our analysis to heterogeneous structures. For generic trees, the critical rewiring threshold scales as

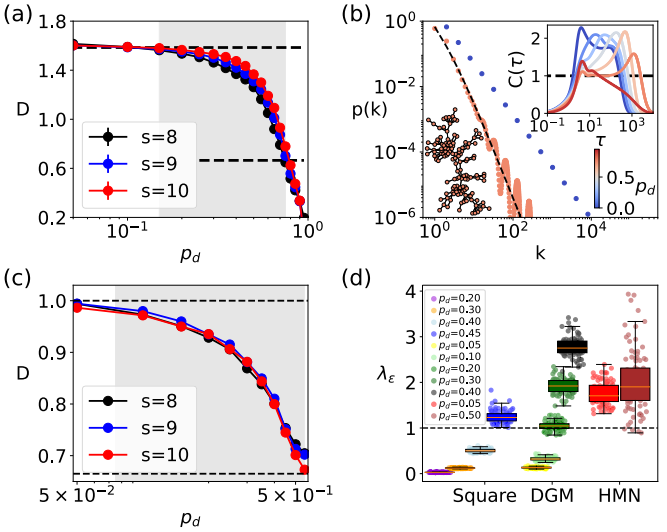

FIG. 3. Diluted scale-invariant networks. (a), (c) Estimated correlation dimension, D, vs dilution probability, p_d, for networks of different generation levels, s (see legend), for (a) DGM ($N_s = \frac{3+3^s}{2}$) and (c) HMN with $m_0 = 3$ and $\alpha = 4$ ($N_s = 2^s m_0$). (b) Degree distribution, $P(\kappa)$, vs node degree, κ, for a DGM network with $p_d = 0$ (blue points) and $p_d = 0.75$ (orange points). The black dashed line indicates the power-law scaling of a BA network, $P(\kappa) \propto \kappa^{-3}$. Inset: Specific heat for different dilution probabilities; for $p_d = 0.75$, the plateau at $C_0 = 1$ confirms the BA limit. (d) Lacunarity index, λ, calculated at a fixed scale $\epsilon = 10^{-2}$ for different network topologies (x axis). Colors distinguish different dilution probabilities (see legend). The horizontal dashed line marks the theoretical reference $\lambda = 1$ (where standard deviation equals mean). All curves have been averaged over 10^3–10^4 realizations.

$p_{r,c} \sim \mathcal{O}(1/N)$, while link deletion leads to a trivial threshold $p_{d,c} = 1$, since the spectral dimension remains unchanged (see Appendix E). In contrast, DGM networks exhibit more significant and nontrivial behavior. For these, we identify nontrivial critical thresholds for rewiring and dilution: $p_{r,c} \neq 0$ (see Appendix D for a discussion on the issue) and $p_{d,c} = 0.15(5)$, respectively (the percolation threshold is $p_c = 0.95(5)$; see Appendix D). Figures 3(a) and 3(c) show the correlation dimension, D, as a function of p_d for DGM and HMN networks. In DGM networks, D remains constant up to $p_{d,c}$ and then begins to decrease. In particular, these networks show evidence of flowing to the vicinity of an unstable structural fixed point for $p_d = 0.75(5)$: As shown in Fig. 3(b), their structure converges to that of a Barabási-Albert (BA) network, following a power-law degree distribution $P(\kappa) \sim \kappa^{-3}$. Furthermore, the heat capacity stabilizes at $C_0 = 1$, matching the BA spectral signature [23,24] [see Fig. 3(b)]. In HMNs (see Appendix F for further analysis), a similar decay in D is observed beyond the corresponding $p_{d,c}$. However, unlike DGM networks, after the percolation threshold, D stabilizes at the RT spectral dimension, $d_s = 4/3$. The absence of hubs prevents the system from flowing close to the BA unstable fixed point reported in the DGM case. Finally, to further characterize the loss of structural regularity, we compute the lacunarity [41,42], λ_ε, or void distribution, defined as the square coefficient of variation of pixels per box in a box-counting analysis: $\lambda_\varepsilon = \frac{\sigma_\varepsilon^2}{\mu_\varepsilon^2}$, with ε the box size. As seen in Fig. 3(d), by using a 3D embedding space, lacunarity increases with dilution across all studied networks. This indicates a breakdown of statistical self-similarity and the emergence of heterogeneity in the spatial complexity. For HMNs, high lacunarity is present even without dilution, indicating their intrinsic geometric irregularity. This is particularly significant because when lacunarity is low, fractals behave similarly to analytically continued hypercubic lattices [43]. Therefore, lacunarity may serve as a signature of anomalous universal behavior.

VI. OUTLOOK

It is generally understood in critical phenomena that once a symmetry of the order parameter and the interaction range are fixed, only the dimension controls the critical properties of the system [44–46]. In the framework of complex networks, this perspective has recently been extended to include scale-invariant networks defined by a well-defined spectral dimension [24]. However, it is unclear how topological noise affects dimensionality in such systems.

Here, we uncover a class of structural phase transitions, which arise in scale-invariant networks and lattices undergoing a critical geometric breakdown under topological perturbations. This allows us to introduce the concept of geometric criticality, occurring when lattices lose translational invariance and networks lose the homogeneous spectral structure. We further demonstrate the existence of attraction basins that depend not only on dimension but also on microscopic structural details, such as the lattice tiling. Topological shortcuts act as local perturbations that induce a global collapse of the underlying manifold once a critical threshold is crossed. Conversely, link dilution erodes dimensional uniformity, leading to multifractal-like geometries. For link dilution, this breakdown also generates high lacunarity values, a measure originally proposed to analyze the deviation of a fractal from being translationally invariant [47], which has been shown to impact critical phenomena on fractal lattices [43].

For HMNs, which are known to exhibit Griffiths phases due to their hierarchical heterogeneity [36], we provide the first evidence of scale-invariant networks that inherently possess high lacunarity, even in the absence of external perturbations. This supports earlier arguments that critical phenomena in fractal systems depend not only on dimension but also on more intricate geometric and topological features. In particular, our framework opens the door to an extensive analysis of Griffiths phases and broad-critical regions from a rigorous perspective.

These geometric transitions, although purely structural in origin, are likely a signature of strong dynamical consequences, potentially altering well-known processes such as transport, synchronization, or memory properties in real systems. We hope that this work will stimulate future research in this direction.

ACKNOWLEDGMENTS

We thank M. A. Muñoz and A. Gabrielli for useful discussions and comments. P.V. acknowledges the Spanish Ministry of Research and Innovation and Agencia Estatal de

TABLE I. Geometric criticality thresholds for structural perturbations. The table reports the critical values for rewiring and dilution processes across various regular lattices and complex network topologies. Parentheses indicate the estimated uncertainty.

	2D square	2D triangular	2D hexagonal	3D cubic	Trees	DGM
Rewiring	0.10(1)	0.17(4)	0.055(10)	0.20(5)	$\mathcal{O}(1/N)$	0.05(3)
Dilution	0.20(5)	0.25(1)	0.11(2)	0.55(5)	1	0.15(5)

Investigación (AEI), MICIN/AEI/10.13039/501100011033, for financial support through Project No. PID2023-149174NB-I00, funded also by European Regional Development Funds, and Ref. PID2020-113681GB-I00.

DATA AVAILABILITY

The data that support the findings of this article are not publicly available. The data are available from the authors upon reasonable request.

APPENDIX A: GEOMETRIC CRITICALITY IN DIFFERENT NETWORKS AND LATTICES

Table I reports the critical values marking the onset of geometric criticality across diverse lattice and network topologies. We examine structural perturbations driven by dilution and rewiring (at conserved link density). These estimates derive from a joint evaluation of the network heat capacity and the correlation dimension, within the limits of the latter's interpretability as detailed in the main text.

APPENDIX B: 2D LATTICES

1. Triangular lattice

We present a detailed analysis of 2D triangular lattices here. Figure 4 reports finite-size scaling analyses confirming the existence of a finite critical rewiring probability in the thermodynamic limit, $p_{r,c} = 0.17(4)$. As in the case of the square lattice, this threshold delimits the attraction basin of the 2D triangular lattice under the introduction of shortcuts. Note that the specific value of $p_{r,c}$ depends on the underlying lattice tiling.

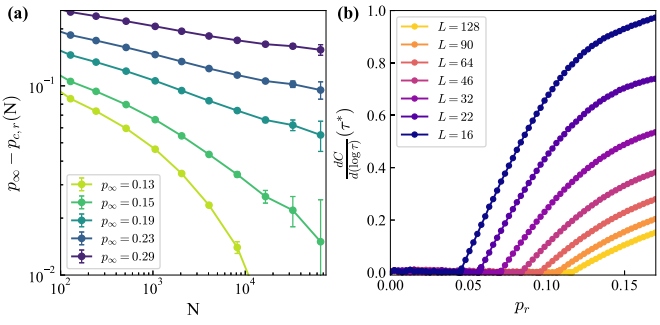

FIG. 4. Criticality in 2D triangular lattices under rewiring. (a) Finite-size scaling of the heat capacity peak locations. The convergence of the size-dependent critical points $p_{r,c}(N)$ toward the asymptotic limit $p_{r,c}^{\infty}$ follows a power law, uniquely identifying the critical threshold at $p_{r,c} = 0.17(4)$ in the thermodynamic limit. (b) First derivative of the heat capacity with respect to the rewiring probability p_r, shown for different lattice sizes (see legend).

In the case of 2D triangular lattices, the heat capacity profile reveals the specific transition point $p_{d,c}$ marking the collapse of the ultraviolet cutoff Λ. This geometric breakdown is signaled by the curvature (concavity) of the first heat capacity peak, illustrated in Figs. 5(a) and 5(b).

Regarding the network topology, Fig. 5(c) reports the correlation dimension as a function of rewiring probability, with the specific scaling exponent $C(\ell) \propto \ell^D$ shown in Fig. 5(d). Crucially, for dilutions exceeding $p_{d,c}$, the effective dimension progressively converges to the Alexander-Orbach (or random tree) value $d_s = 4/3$ at the percolation threshold p_c.

2. Hexagonal lattice

Turning to the 2D hexagonal lattice, the finite-size scaling analysis in Fig. 6 confirms the existence of a finite critical rewiring probability in the thermodynamic limit, $p_{r,c} = 0.055(10)$. As observed for square and triangular lattices, this threshold delimits the attraction basin of the hexagonal geometry against the introduction of shortcuts. These results

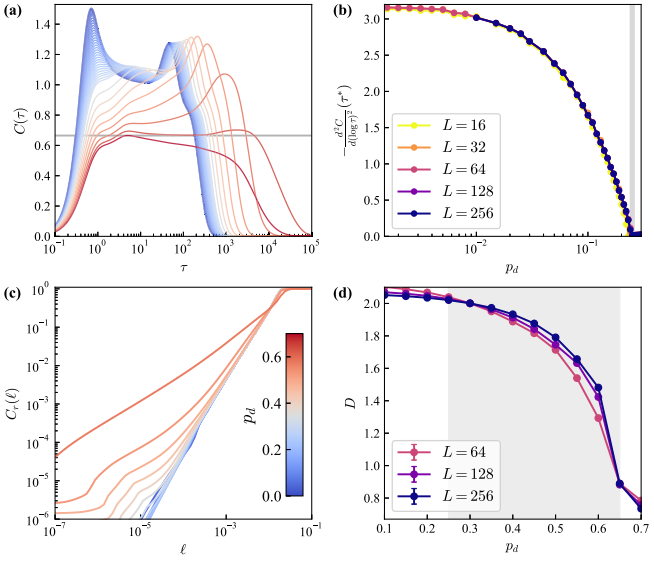

FIG. 5. Geometric breakdown of 2D triangular lattices under dilution. (a) Heat capacity C as a function of diffusion time τ for varying dilution probabilities (see colorbar). The gray line marks the Alexander-Orbach (RT) plateau. (b) Second derivative (curvature) of the heat capacity at the first peak vs dilution probability p_d for different lattice sizes. The vertical gray line indicates the critical point where the 2D ultraviolet cutoff vanishes. (c) Correlation integral $C_r(\ell)$ vs distance ℓ for different dilution probabilities. (d) Estimated correlation dimension D vs p_d for different lattice sizes. The gray shaded region marks the regime between $p_{d,c}$ and the percolation threshold. All curves represent averages over 10^3–10^4 realizations.

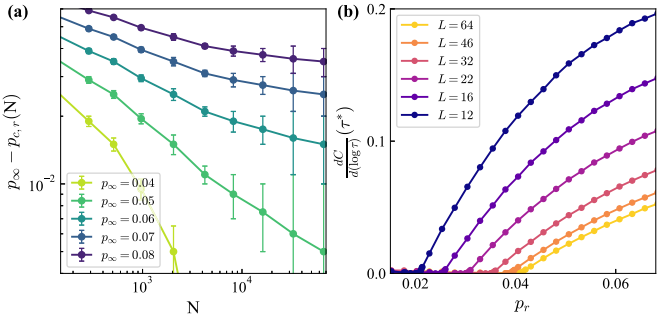

FIG. 6. Criticality in 2D hexagonal lattices under rewiring. (a) Finite-size scaling of the heat capacity peak locations. The convergence of the size-dependent critical points $p_{r,c}(N)$ toward the asymptotic limit $p_{r,c}^{\infty}$ follows a power law, uniquely identifying the critical threshold at $p_{r,c}^{\infty} = 0.055(10)$. (b) First derivative of the heat capacity with respect to the rewiring probability p_r, shown for different lattice sizes (see legend).

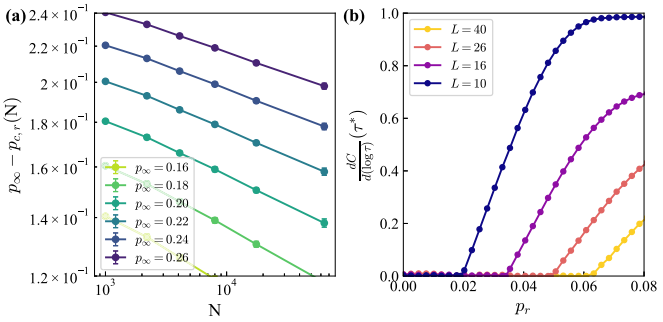

FIG. 8. Criticality in 3D cubic lattices under rewiring. (a) Finite-size scaling of the heat capacity peak locations. The convergence of the size-dependent critical points $p_{r,c}(N)$ toward the asymptotic limit $p_{r,c}^{\infty}$ follows a power law, uniquely identifying the critical threshold at $p_{r,c}^{\infty} = 0.20(5)$. (b) First derivative of the heat capacity with respect to the rewiring probability p_r, shown for different lattice sizes (see legend).

further illustrate that the specific value of $p_{r,c}$ is intrinsically dependent on the lattice tiling.

For 2D hexagonal lattices, the analysis of the heat capacity as a function of the dilution probability identifies the critical point $p_{d,c}$ at which the ultraviolet cutoff Λ vanishes. We detect this geometric breakdown by analyzing the concavity of the first heat capacity peak [see Fig. 7(a)], as detailed in Fig. 7(b).

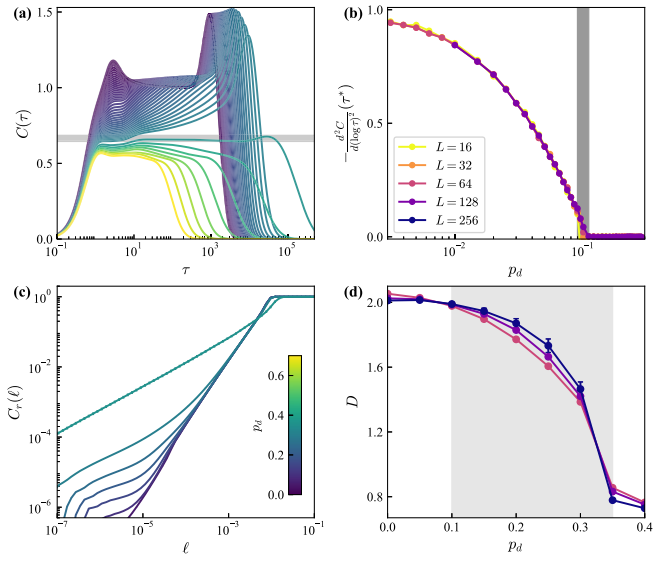

FIG. 7. Geometric breakdown of 2D hexagonal lattices under dilution. (a) Heat capacity C as a function of diffusion time τ for varying dilution probabilities (see colorbar). The gray line marks the Alexander-Orbach (RT) plateau. (b) Second derivative (curvature) of the heat capacity at the first peak vs dilution probability p_d for different lattice sizes. The vertical gray line indicates the critical point where the 2D ultraviolet cutoff vanishes. (c) Correlation integral $C_r(\ell)$ vs distance ℓ for different dilution probabilities. (d) Estimated correlation dimension D vs p_d for different lattice sizes. The gray shaded region marks the regime between $p_{d,c}$ and the percolation threshold. All curves represent averages over 10^3–10^4 realizations.

Figure 7(c) presents the correlation dimension under rewiring, while Fig. 7(d) plots the dimension derived from the scaling $C(\ell) \propto \ell^D$. Notably, beyond $p_{d,c}$, the effective dimension decreases progressively toward the RT value $d_s = 4/3$ at p_c.

APPENDIX C: 3D LATTICES

Extending our analysis to three dimensions, Fig. 8 illustrates the impact of shortcuts on cubic lattices. Finite-size scaling confirms the existence of a critical rewiring threshold at $p_{r,c} = 0.20(5)$ in the thermodynamic limit. This value marks the boundary of the lattice's attraction basin, analogous to the 2D cases. These results reinforce the observation that the critical point is intrinsically linked to the specific lattice geometry.

For 3D cubic lattices, analyzing the heat capacity as a function of the dilution probability identifies the critical point $p_{d,c}$ at which the ultraviolet cutoff Λ vanishes. We detect this geometric breakdown by examining the concavity of the first heat capacity peak, as illustrated in the left panel of Fig. 9. Figure 9 also presents the correlation dimension under rewiring, while the specific dimension extracted from the scaling $C(\ell) \propto \ell^D$ is reported in the rightmost panel. Notably, beyond $p_{d,c}$, the effective dimension of the network progressively decreases toward the random tree (RT) value $d_s = 4/3$ at p_c.

APPENDIX D: DGM NETWORKS

We now move to the case of DGM networks under rewiring, as shown in Fig. 10. Finite-size scaling analyses confirm the existence of a finite critical rewiring probability in the thermodynamic limit, estimated at $p_{r,c} = 0.05(3)$.

Specifically, we observe that assuming an asymptotic limit of $p_{r,c}^{\infty} = 0.03$ yields a consistent convergence to zero as system size increases. In contrast, setting $p_{r,c}^{\infty} = 0.02$ results in an exponential decay with system size. This behavior establishes the attraction basin for this scale-invariant network against shortcut perturbations.

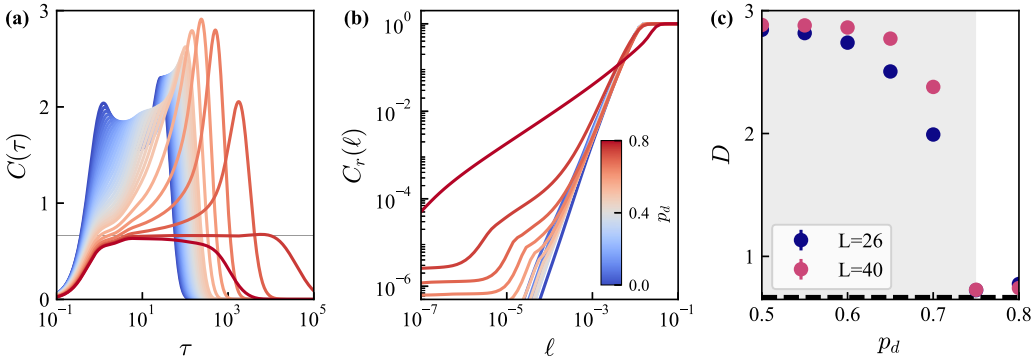

FIG. 9. Geometric breakdown of 3D cubic lattices under dilution. (a) Heat capacity C vs diffusion time τ for varying dilution probabilities (see colorbar). The gray line marks the Alexander-Orbach (RT) plateau. (b) Correlation integral $C_r(\ell)$ as a function of distance ℓ for different dilution probabilities. (c) Estimated correlation dimension D vs dilution probability p_d for different lattice sizes. The gray shaded region marks the interval between $p_{d,c}$ and the percolation threshold. All curves represent averages over 10^3–10^4 realizations.

Figure 11 displays the correlation integral for different dilution probabilities in a DGM network of size $N = 29\,526$. In the low-dilution regime, the network exhibits a spectral dimension consistent with the expected theoretical value. However, as dilution increases, this dimension progressively deviates, eventually signaling a structural collapse.

Figure 12 reports the percolation properties of diluted DGM networks. The left panel displays the average fraction of nodes belonging to the giant component as a function of dilution probability for varying hierarchical levels s (see legend).

As dilution increases, the giant component progressively decreases, suggesting a percolation threshold approaching one. Complementarily, the standard deviation of the percolation order parameter highlights the fluctuations associated with the phase transition. The peak of these fluctuations identifies the true critical point at $p_c = 0.95(5)$. Furthermore, finite-size scaling analysis across different values of s confirms that the critical threshold remains strictly below one.

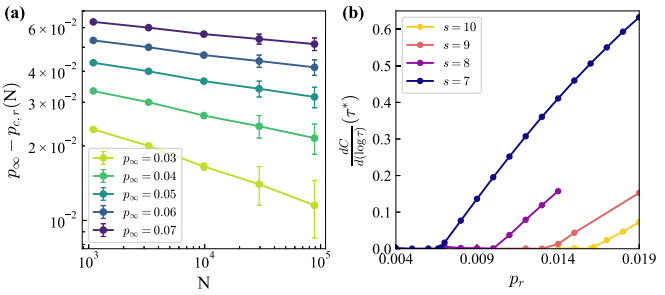

FIG. 10. Criticality in DGM networks under rewiring. (a) Finite-size scaling of the heat capacity peak locations. The convergence of the size-dependent critical points $p_{r,c}(N)$ toward the asymptotic limit $p_{r,c}^{\infty}$ follows a power law, uniquely identifying the critical threshold at $p_{r,c}^{\infty} = 0.05(3)$. (b) First derivative of the heat capacity with respect to the rewiring probability p_r, shown for different generation levels s (see legend).

APPENDIX E: TREE NETWORKS

Here, we report the percolation transition as a function of rewiring probability for random trees and Barabási-Albert networks. Structurally, these systems are analogous to one-dimensional (1D) rings because they lack loops. Notably, in all three cases, the critical probability required to sustain a giant connected component vanishes in the thermodynamic limit. This behavior is confirmed by the data collapse observed when the curves are properly rescaled with N, as illustrated in Fig. 13.

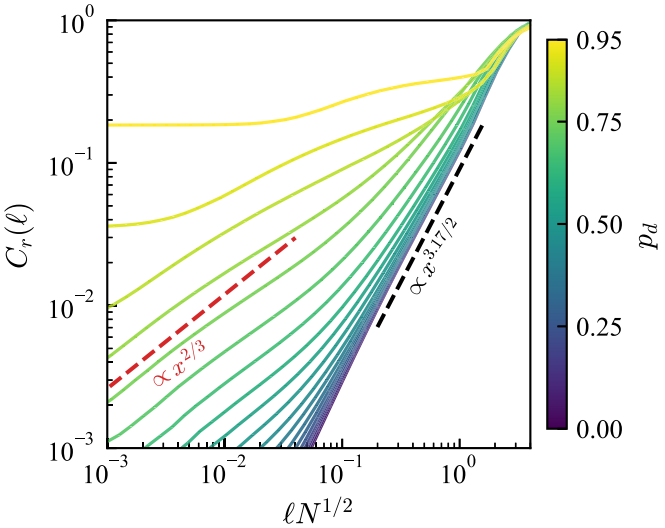

FIG. 11. Scaling analysis of DGM networks. Correlation integral $C_r(\ell)$ as a function of the rescaled distance $\ell\sqrt{N}$ for networks at generation level $s = 10$, subjected to varying dilution probabilities (see legend). Dashed lines serve as guides to the eye, indicating slopes corresponding to correlation dimensions $D = 2/3$ (red dashed line) and $D = 3.17/2$ (blue dashed line).

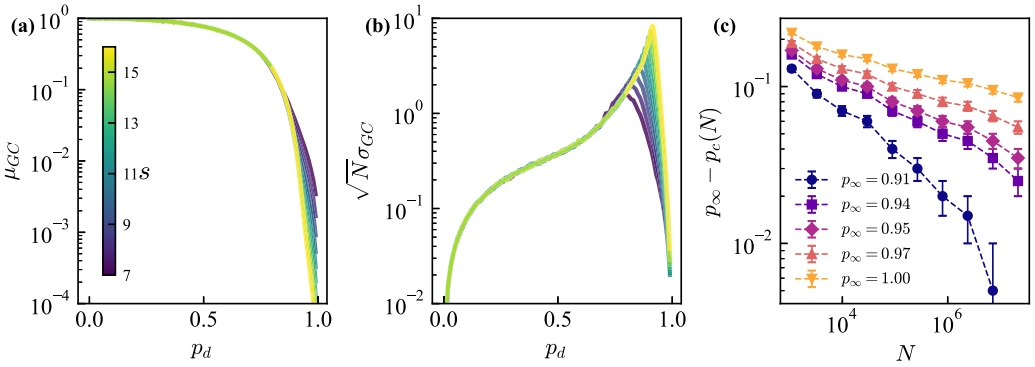

FIG. 12. Percolation transition in DGM networks. (a) Average fraction of nodes in the giant component as a function of dilution probability for varying generation levels s (see legend). (b) Standard deviation of the giant component fraction, representing the order parameter fluctuations across different levels s. (c) Finite-size scaling analysis of the percolation threshold $p_c(s)$ vs system size.

APPENDIX F: HIERARCHICAL MODULAR NETWORKS

Finally, Fig. 14 illustrates the percolation behavior of diluted HMNs across varying hierarchical levels s. The left panel depicts the average fraction of nodes in the giant component as a function of dilution probability. As dilution increases, the network undergoes a complex percolation transition. Crucially, the analysis of the susceptibility (defined as the standard deviation of the order parameter; see center panel) reveals a broad critical region, with fluctuations that appear to diverge in the thermodynamic limit even at low values of p_d. This suggests the presence of persistent critical fluctuations associated with the network's specific lacunarity across the entire dilution range. Finally, the right panel reports the heat capacity C as a function of diffusion time τ for varying dilution probabilities (see colorbar).

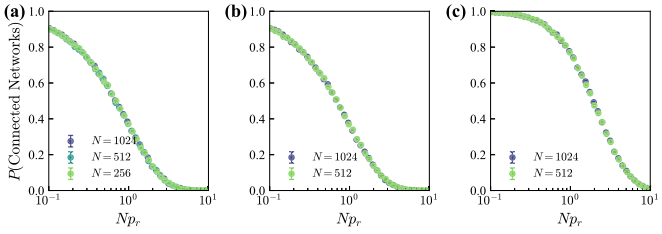

FIG. 13. Connectivity transition in loop-free topologies. Probability of observing a fully connected network as a function of the rescaled rewiring probability $p_r N$. (a) Barabási-Albert networks with $m = 1$. (b) Random trees. (c) Ring graphs (1D lattices). Different curves correspond to different system sizes N (see legend).

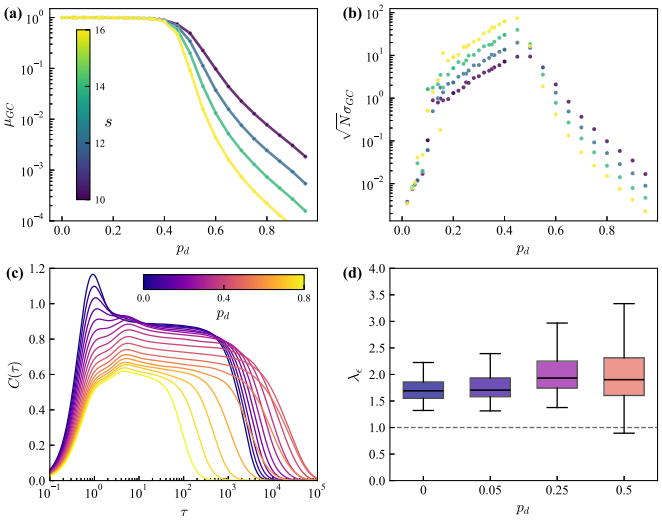

FIG. 14. Percolation and heat capacity analysis in diluted HMNs. (a) Average fraction of nodes in the giant component as a function of dilution probability p_d. Different curves correspond to different hierarchical levels s (see legend). (b) Standard deviation of the giant component fraction, representing order parameter fluctuations vs p_d for different levels s. (c) Heat capacity C vs diffusion time τ for varying dilution probabilities (see colorbar). (d) Lacunarity index, λ_ϵ, calculated at a fixed scale $\epsilon = 10^{-2}$, for diluted HMN with $m_0 = 3$, $\alpha = 4$, and $s = 11$. The horizontal dashed line marks the theoretical reference $\lambda_\epsilon = 1$.

[1] R. F. Betzel and D. S. Bassett, Specificity and robustness of long-distance connections in weighted, interareal connectomes, Proc. Natl. Acad. Sci. USA **115**, E4880 (2018).

[2] P. Martin, A. McGovern, G. Orozco, *et al.*, Capture Hi-C reveals novel candidate genes and complex long-range interactions with related autoimmune risk loci, Nat. Commun. **6**, 10069 (2015).

[3] A. Simonov and A. L. Goodwin, Designing disorder into crystalline materials, Nat. Rev. Chem. **4**, 657 (2020).

[4] O. Sporns, *Networks of the Brain* (MIT Press, Cambridge, MA, 2010).

[5] M. Kaiser and C. C. Hilgetag, Nonoptimal component placement, but short processing paths, due to long-distance projections in neural systems, PLoS Comput. Biol. **2**, e95 (2006).

[6] E. Bullmore and O. Sporns, Complex brain networks: Graph theoretical analysis of structural and functional systems, Nat. Rev. Neurosci. **10**, 186 (2009).

[7] R. F. Betzel and D. S. Bassett, Multi-scale brain networks, NeuroImage **160**, 73 (2017).

[8] F. Schein and P. C. Aichelburg, Traversable wormholes in geometries of charged shells, Phys. Rev. Lett. **77**, 4130 (1996).

[9] Y.-C. Chen, Z.-G. Huang, and Y.-C. Lai, Controlling extreme events on complex networks, Sci. Rep. **4**, 6121 (2014).

[10] R. E. Morris and J. Čejka, Exploiting chemically selective weakness in solids as a route to new porous materials, Nat. Chem. **7**, 381 (2015).

[11] W. J. Roth, *et al.*, A family of zeolites with controlled pore size prepared using a top-down method, Nat. Chem. **5**, 628 (2013).

[12] Z. Zhang, F. Zuo, C. Wan, A. Dutta, J. Kim, J. Rensberg, R. Nawrodt, H. H. Park, T. J. Larrabee, X. Guan, Y. Zhou, S. M. Prokes, C. Ronning, V. M. Shalaev, A. Boltasseva, M. A. Kats, and S. Ramanathan, Evolution of metallicity in vanadium dioxide by creation of oxygen vacancies, Phys. Rev. Appl. **7**, 034008 (2017).

[13] J. J. Brown, Y. Shao, Z. Ke, and A. J. Page, Anion vacancy effects on structural stability in oxynitrides, Mater. Adv. **2**, 2398 (2021).

[14] J. Zhou, Vacancy defects in skyrmion crystals: Structural and magnetic effects, J. Magn. Magn. Mater. **562**, 170147 (2023).

[15] D. J. Watts and S. H. Strogatz, Collective dynamics of 'small-world' networks, Nature (London) **393**, 440 (1998).

[16] M. Newman and D. Watts, Renormalization group analysis of the small-world network model, Phys. Lett. A **263**, 341 (1999).

[17] M. E. J. Newman, Models of the small world, J. Stat. Phys. **101**, 819 (2000).

[18] A. P. Millán, G. Gori, F. Battiston, T. Enss, and N. Defenu, Complex networks with tuneable spectral dimension as a universality playground, Phys. Rev. Res. **3**, 023015 (2021).

[19] T. Vojta, Rare region effects at classical, quantum and nonequilibrium phase transitions, J. Phys. A: Math. Gen. **39**, R143 (2006).

[20] R. B. Griffiths, Nonanalytic behavior above the critical point in a random Ising ferromagnet, Phys. Rev. Lett. **23**, 17 (1969).

[21] V. Westphal, W. Kleemann, and M. D. Glinchuk, Diffuse phase transitions and random-field-induced domain states of the "relaxor" ferroelectric $PbMg_{1/3}Nb_{2/3}O_3$, Phys. Rev. Lett. **68**, 847 (1992).

[22] P. Timonin, Griffiths' phase in dilute ferroelectrics, Ferroelectrics **199**, 69 (1997).

[23] P. Villegas, T. Gili, G. Caldarelli, and A. Gabrielli, Laplacian renormalization group for heterogeneous networks, Nat. Phys. **19**, 445 (2023).

[24] A. Poggialini, P. Villegas, M. A. Muñoz, and A. Gabrielli, Networks with many structural scales: A renormalization group perspective, Phys. Rev. Lett. **134**, 057401 (2025).

[25] D. Cassi, Local vs average behavior on inhomogeneous structures: Recurrence on the average and a further extension of Mermin-Wagner theorem on graphs, Phys. Rev. Lett. **76**, 2941 (1996).

[26] D. Cassi, Phase transitions and random walks on graphs: A generalization of the Mermin-Wagner theorem to disordered lattices, fractals, and other discrete structures, Phys. Rev. Lett. **68**, 3631 (1992).

[27] P. Villegas, Strange attractors in complex networks, Phys. Rev. E **111**, L042301 (2025).

[28] A. Gabrielli, D. Garlaschelli, S. Patil, *et al.*, Network renormalization, Nat. Rev. Phys. **7**, 203 (2025).

[29] M. De Domenico and J. Biamonte, Spectral entropies as information-theoretic tools for complex network comparison, Phys. Rev. X **6**, 041062 (2016).

[30] P. Villegas, A. Gabrielli, F. Santucci, G. Caldarelli, and T. Gili, Laplacian paths in complex networks: Information core emerges from entropic transitions, Phys. Rev. Res. **4**, 033196 (2022).

[31] L. Falsi, P. Villegas, T. Gili, A. J. Agranat, and E. DelRe, Topological protection breakdown: A route to frustrated ferroelectricity, Phys. Rev. Res. **7**, 043038 (2025).

[32] L. Donetti and C. Destri, The statistical geometry of scale-free random trees, J. Phys. A: Math. Gen. **37**, 6003 (2004).

[33] H. D. Rozenfeld, S. Havlin, and D. Ben-Avraham, Fractal and transfractal recursive scale-free nets, New J. Phys. **9**, 175 (2007).

[34] S. N. Dorogovtsev, A. V. Goltsev, and J. F. F. Mendes, Pseudofractal scale-free web, Phys. Rev. E **65**, 066122 (2002).

[35] P. Holme and B. J. Kim, Growing scale-free networks with tunable clustering, Phys. Rev. E **65**, 026107 (2002).

[36] P. Moretti and M. A. Muñoz, Griffiths phases and the stretching of criticality in brain networks, Nat. Commun. **4**, 2521 (2013).

[37] See Supplemental Material at http://link.aps.org/supplemental/10.1103/75gt-z6x6 for videos supporting the findings in the main text.

[38] S. Alexander and R. Orbach, Density of states on fractals: 'Fractons', J. Physique Lett. **43**, 625 (1982).

[39] P. Grassberger and I. Procaccia, Measuring the strangeness of strange attractors, Physica D **9**, 189 (1983).

[40] P. Villegas, T. Gili, G. Caldarelli, and A. Gabrielli, Evidence of scale-free clusters of vegetation in tropical rainforests, Phys. Rev. E **109**, L042402 (2024).

[41] B. B. Mandelbrot, *The Fractal Geometry of Nature*, revised and enlarged ed. (W. H. Freeman and Co., New York, 1983), p. 495.

[42] A. Gabrielli, F. S. Labini, M. Joyce, and L. Pietronero, *Statistical Physics for Cosmic Structures* (Springer Science & Business Media, New York, 2006).

[43] Y. Gefen, Y. Meir, B. B. Mandelbrot, and A. Aharony, Geometric implementation of hypercubic lattices with noninteger dimensionality by use of low lacunarity fractal lattices, Phys. Rev. Lett. **50**, 145 (1983).

[44] J. J. Binney, N. J. Dowrick, A. J. Fisher, and M. E. Newman, *The Theory of Critical Phenomena: An Introduction to the Renormalization Group* (Oxford University Press, Oxford, 1992).

[45] D. J. Amit and V. Martin-Mayor, *Field Theory, the Renormalization Group, and Critical Phenomena*, 3rd ed. (World Scientific, Singapore, 2005).

[46] L. P. Kadanoff, in *Proceedings of the Enrico Fermi Summer School of Physics, Varenna 1970*, edited by M. S. Green (Academic Press, London/New York, 1971), chap. 2, pp. 100–117.

[47] Y. Gefen, B. B. Mandelbrot, and A. Aharony, Critical phenomena on fractal lattices, Phys. Rev. Lett. **45**, 855 (1980).